Giretti, D. *et al.* (2020). *Géotechnique* **70**, No. 10, 937–942 [https://doi.org/10.1680/jgeot.18.D.014]

DISCUSSION

Mechanical properties of a carbonate sand from a dredged hydraulic fill

D. GIRETTI*, V. FIORAVANTE†, K. BEEN‡, S. DICKENSON§, G. MESRI‖ and T. KANE‖

Contribution by G. Mesri and T. Kane

The 'Mechanical properties of a carbonate sand from a dredged hydraulic fill' (Giretti *et al.*, 2018a) together with its companion paper 'CPT calibration and analysis for a carbonate sand' (Giretti *et al.*, 2018b) are valuable because there are limited data in the literature on biogenic carbonate sands. 'Compression of granular materials' by Mesri & Vardhanabhuti (2009) includes some data on carbonate sands. In laterally constrained compression or isotropic compression, carbonate sands display a type C void ratio against effective stress behaviour for which significant level I and level II particle damage begin at low effective stresses and continue with or without gradual level III particle damage at higher stresses. Level I particle damage includes abrasion or grinding of particle surface asperities, level II particle damage includes breaking or crushing of particle surface protrusions and sharp particle corners and edges, and level III particle damage includes fracturing, splitting or shattering of particles.

The void ratio plotted against effective stress relationships of most space-lattice silicate sands displays three distinct stages of compression. During the first stage, small particle movements further engage particle surface roughness and enhance interparticle locking. There is minor to small level I and level II particle damage; however, improved locking dominates over unlocking effects and $M = \Delta\sigma'_v/\Delta\varepsilon_v$ increases with the increase in σ'_v. The second compression stage begins with level III particle damage by the fracturing of the heavily loaded particles and collapse of the load-bearing aggregate framework. Particle fracturing unlocks the aggregate framework, allowing larger interparticle movements and M begins to decrease with an increase in σ'_v (see, for examples, Figs 2 and 22 in the paper by Mesri & Vardhanabhuti (2009)). The first inflection point in the e plotted against σ'_v relationship marks the beginning of the second stage at an effective vertical stress $(\sigma'_v)_{M_{max}}$, and a second inflection point at $(\sigma'_v)_{M_{min}}$ marks the end at which major particle fracturing and splitting are substantially complete. In the void ratio plotted against logarithm of effective stress relationship of most sands, it is possible to identify a point of maximum curvature at $(\sigma'_v)_{MC}$ (see, for example, Figs 2 and 22 in the paper by Mesri & Vardhanabhuti (2009)).

Because in type C void ratio plotted against effective stress compression behaviour, significant level I and level II particle damage begin early at low effective stresses and continue with or without gradual level III particle damage at high stresses, the void ratio against effective stress relationship, such as that in Fig. 18(b) for M1 carbonate sand (from Fig. 3 of Giretti *et al.* (2018a)), does not display three distinct stages of compression. However, for some carbonate sands examined by Mesri & Vardhanabhuti (2009), it was possible to extract values of $(\sigma'_v)_{MC}$, $(\sigma'_v)_{M_{max}}$ and $(\sigma'_v)_{M_{min}}$, leading to $(\sigma'_v)_{M_{max}} = 0{\cdot}67(\sigma'_v)_{MC}$ and $(\sigma'_v)_{M_{min}} = 2{\cdot}0(\sigma'_v)_{MC}$. In Fig. 18(a), a value of $(\sigma'_v)_{MC} = 1$ MPa was selected for M1 carbonate sand, and the values of $(\sigma'_v)_{M_{max}}$ and $(\sigma'_v)_{M_{min}}$ were computed only for reference, as it is not possible to identify them on Fig. 18(b). A main difference between the compression behaviour of carbonate sands as compared to that of silicate sands, is that, for the data examined by Mesri & Vardhanabhuti (2009), for carbonate sands the values of $(\sigma'_v)_{MC}$ are in the range of 0·4–2 MPa, whereas for silicate sands, they are in the range of 4–40 MPa (Fig. 21 of Mesri & Vardhanabhuti (2009)).

According to cone penetration tests in calibration chambers, and interpretation by Houlsby & Hitchman (1988), for silicate sands, cone tip resistance, q_t, is governed primarily by effective horizontal stress, σ'_h, according to

$$\frac{q_t}{p_a} = A\left(\frac{\sigma'_h}{p_a}\right)^{0{\cdot}6} \tag{6}$$

in which p_a is atmospheric pressure, and parameter A had values of 50, 160 and 230, respectively, for loose, medium and dense silicate sands.

Based on the K_0 versus σ'_v measurements in Fig. 12, the authors selected an average value of $K_0 = 0{\cdot}5$ for the M1 carbonate sand with void ratio in the range of 0·58–0·89. Because σ'_h, and thus K_0 as a function of void ratio, is a significant factor in cone tip resistance according to equation (6), in Fig. 19 the K_0 values from Fig. 12 have been plotted for the M1 carbonate sand against void ratio. The extrapolation, in Fig. 19, of the data to initial void ratio of M1 carbonate sand (Fig. 3, M1 small oedometer) leads to a $K_0 = 0{\cdot}36$. According to Mesri & Hayat (1993), the Jaky (1948) equation for K_{0p} is

$$K_{0p} = 1 - \sin\phi'_{cv} \tag{7}$$

which together with $\phi'_{cv} = 40{\cdot}3°$ leads to $K_{0p} = 0{\cdot}36$. Note that for Mexico City clay with poriferous diatom shells, $\phi'_{cv} = 43°$ and measured $K_{0p} = 0{\cdot}30$ (Mesri *et al.*, 1975; Mesri & Hayat, 1993). For comparison with behaviour of the M1 carbonate sand, Fig. 20 shows K_0 plotted against void ratio for three silicate sands which were densified by vibration (Mesri & Vardhanabhuti, 2007).

The discussers have interpreted, and shown in Table 3, the cone tip resistance, q_t, in dry M1 sand in Fig. 12, of Giretti *et al.* (2018b) using equation (6) together with K_0 in Fig. 19. The computed values of parameter A, ranging from an average value 110 at $e = 0{\cdot}823$ to 259 at $e = 0{\cdot}666$, are plotted in Fig. 19. Values of ϕ'_{tc} for the M1 carbonate sand have also been computed, as listed in Table 3, by means of the empirical equation reported by Houlsby & Hitchman (1988) for silicate sands

$$\ln N_h = 0{\cdot}16\,(\phi'_{tc} - 9) \tag{8}$$

where $N_h = q_t/\sigma'_h$. Most of the computed magnitudes of ϕ'_{tc}, only several degrees higher than $\phi'_{cv} = 40{\cdot}3°$, are reasonable because the highly crushable calcium carbonate particles cannot mobilise significant dilatant geometrical interference beyond $\phi'_{cv} = 40{\cdot}3°$. However, for one q_t measurement at $e = 0{\cdot}727$ and four q_t measurements at $e = 0{\cdot}823$, the

* ISMGEO srl, Seriate, Bergamo, Italy (Orcid:0000-0003-4145-1388).
† University of Ferrara, Ferrara, Italy.
‡ Golder Associates Ltd, Halifax, NS, Canada.
§ New Albion Geotechnical Inc., Reno, NV, USA.
‖ University of Illinois, Urbana-Champaign, IL, USA.

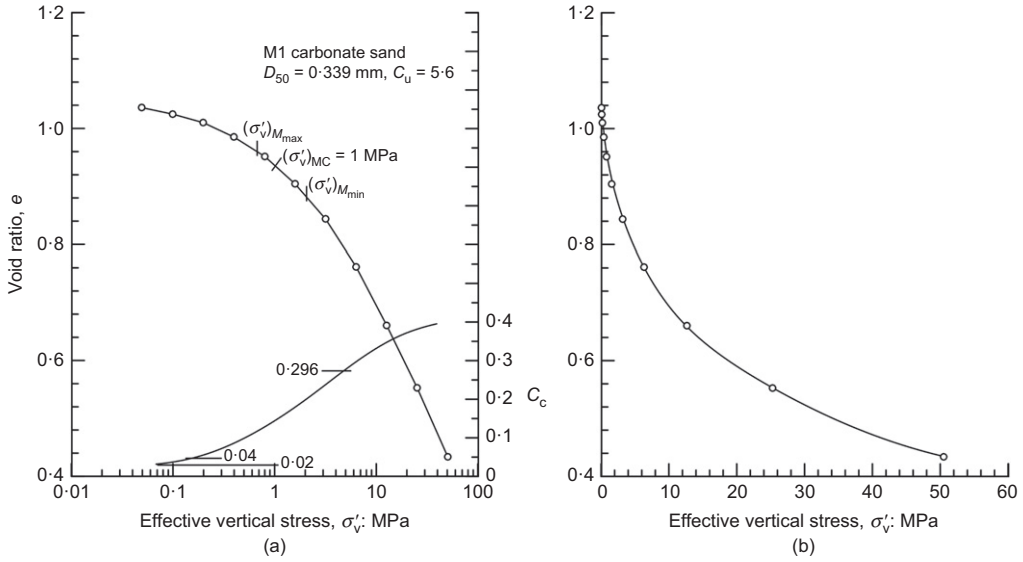

Fig. 18. Void ratio plotted against logarithm of σ'_v and void ratio plotted against σ'_v for M1 carbonate sand; $(\sigma'_v)_{M_{max}}$ and $(\sigma'_v)_{M_{min}}$ computed using $(\sigma'_v)_{M_{max}}/(\sigma'_v)_{MC} = 0{\cdot}67$ and $(\sigma'_v)_{M_{min}}/(\sigma'_v)_{MC} = 2{\cdot}0$; values of $C_c = \Delta e/\Delta \log \sigma'_v$ mentioned in the paper by Giretti *et al.* (2018a) are marked for reference

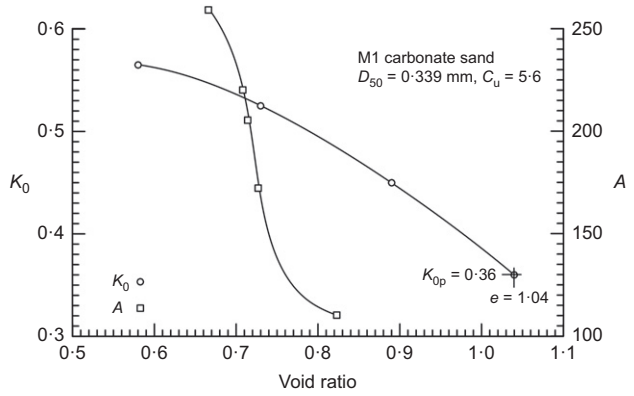

Fig. 19. Relationships between K_0 and parameter A with void ratio for M1 carbonate sand

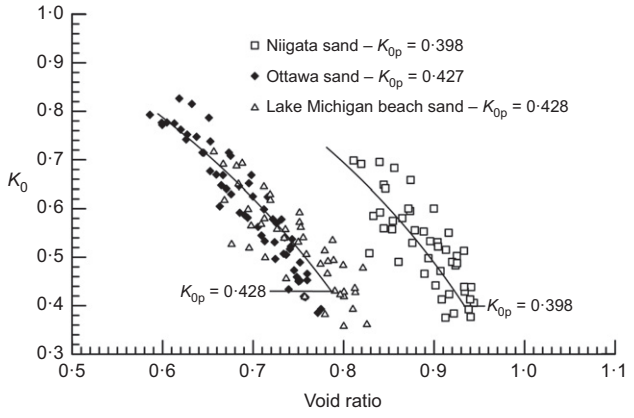

Fig. 20. Relationship between K_0 and void ratio for three silicate sands densified by vibration

computed values of ϕ'_{tc} are actually smaller than $\phi'_{cv} = 40{\cdot}3°$. Apparently, for these combinations of void ratio and effective stress condition in M1 carbonate sand with crushable particles, the ϕ'_p component of friction angle resulting from interparticle interference during shear is smaller than the magnitude mobilised at a constant volume shearing condition (Terzaghi *et al.*, 1996).

Table 3. Interpretation of cone tip resistance measured in dry M1 carbonate sand in Fig. 12 of Giretti *et al.* (2018b) by equation (6) together with K_0 in Fig. 19

q_t: MPa	σ'_v: kPa	σ'_h: kPa	A	N_h	ϕ'_{tc}: degrees
$e = 0{\cdot}666$					
17·5	94·6	51·5	261	340·6	45·4
21·4	129·9	70·7	264	303·1	44·7
24·2	153·9	83·8	269	288·8	44·4
26·4	193·4	105·3	256	250·8	43·5
27·7	224·5	122·2	246	227·0	42·9
$e = 0{\cdot}708$					
15·9	91·8	48·7	245	326·5	45·2
17·1	116·5	61·9	229	277·2	44·2
20·0	136·2	72·3	243	276·4	44·1
22·1	173·6	92·2	232	239·3	43·2
22·0	199·1	105·7	213	208·3	42·4
21·0	221·6	117·7	190	178·3	41·4
22·6	254·1	135·0	189	167·5	41·0
$e = 0{\cdot}714$					
12·5	84·0	44·4	204	281·6	44·3
14·1	108·0	57·1	197	246·6	43·4
17·0	127·8	67·6	216	252·2	43·6
19·2	148·2	78·4	222	245·0	43·4
20·9	176·5	93·4	218	223·7	42·8
21·9	201·2	106·4	211	205·5	42·3
20·9	220·9	116·9	191	179·1	41·4
22·6	255·5	135·2	189	167·3	41·0
25·2	273·2	144·5	202	174·5	41·3
$e = 0{\cdot}727$					
9·6	76·2	40·0	166	239·0	43·2
10·7	98·1	51·5	159	207·7	42·4
13·7	133·4	70·0	170	196·4	42·0
15·8	151·3	79·3	181	198·9	42·1
16·9	164·5	86·3	184	195·5	42·0
17·6	180·9	94·9	181	185·0	41·6
18·3	187·5	98·3	185	186·5	41·7
18·2	232·2	121·8	161	149·2	40·3
19·7	266·6	139·8	161	140·8	39·9
$e = 0{\cdot}823$					
7·2	88·2	42·8	119	167·7	41·0
8·0	118·8	57·6	111	138·8	39·8
8·9	142·8	69·3	111	128·2	39·3
9·9	183·8	89·1	106	111·1	38·4
11·1	218·6	106·0	107	104·2	38·0
12·1	253·9	123·1	107	98·3	37·7

Values of ϕ'_{tc} were estimated using equation (8).

Authors' reply

The authors thank the discussion contributors for their very interesting observations, which provided the possibility of further analysing some aspects of the mechanical behaviour of carbonate sands.

The authors acknowledge the observation that M1 sand shows a type C void ratio–effective stress behaviour, with a progressive increase of the constrained modulus M.

As to the interpretation of the centrifuge cone penetration tests (CPTs) on M1, the basic concept of the authors' analysis is that both the stress-dilatancy behaviour and the normalised cone resistance of M1 sand depend on the state parameter ψ.

This is shown

(*a*) in Fig. 8 of Giretti *et al.* (2018a) where the peak shearing resistance angle is plotted against ψ; the trend ϕ'_{tc}–ψ can be expressed with a linear function a

$$\phi'_{tc} = \phi'_{cs} - a\,\psi \tag{9}$$

where $\phi'_{cs} = 40{\cdot}3°$ is M1 shearing resistance angle at critical state and $a = 25{\cdot}5$ is the function slope.

(*b*) in Figs 16–18 of Giretti *et al.* (2018b), where the normalised cone resistance $Q_p = (q_t - p)/p'$ is plotted against ψ; an exponential function has been adopted to interpret the experimental trend

$$Q_p = k\,\exp(-m\psi) \tag{10}$$

where k and m are calibration coefficients whose values are 42 and 5·1 for dry M1 sand and 35 and 5·1 for saturated M1 sand.

From the data in Table 3, ϕ'_{tc} has been recomputed according to equations (9) and (10). The recomputed values are listed in Table 4; they are slightly larger than ϕ'_{cs} in the looser sample, up to 9° higher than ϕ'_{cs} in the denser sample.

The difference between the ϕ'_{tc} values computed by the contributors and the authors' estimation could be due to the value of the constants Q and R of the stress-dilatancy model of Bolton (1986), on which the Houlsby & Hitchman (1988) $q_t/\sigma'_h - \phi'_{tc}$ equation is based – constants which were calibrated for silica sand. According to the Bolton (1986) model, Q is a particle strength parameter equal to 10 for quartz sands and R is normally assumed as equal to 1.

In Fig. 21 the difference $\phi'_{tc} - \phi'_{cs}$ computed for M1 sand is represented as a function of the relative density D_r (data from Fig. 8 in the paper by Giretti *et al.* (2018a)); in the figure, the

Table 4. Peak shear angle from CPTs in dry M1 sand

Giretti *et al.* (2018a)		Contribution by Mesri and Kane (Table 3)				Authors' reply			
q_t: MPa	σ'_v: kPa	σ'_h: kPa	A	N_h	ϕ'_{tc}: degrees	p': kPa	Q_p	ψ	ϕ'_{tc}: degrees
$e = 0{\cdot}666$									
17·5	94·6	51·5	261	340·6	45·4	65·87	264·69	−0·36	49·5
21·4	129·9	70·7	264	303·1	44·7	90·43	235·64	−0·34	48·9
24·2	153·9	83·8	269	288·8	44·4	107·17	224·82	−0·33	48·7
26·4	193·4	105·3	256	250·8	43·5	134·67	195·04	−0·30	48·0
27·7	224·5	122·2	246	227	42·9	156·30	176·22	−0·28	47·5
$e = 0{\cdot}708$									
15·9	91·8	48·7	245	326·5	45·2	63·07	251·11	−0·35	49·3
17·1	116·5	61·9	229	277·2	44·2	80·10	212·48	−0·32	48·4
20	136·2	72·3	243	276·4	44·1	93·60	212·68	−0·32	48·4
22·1	173·6	92·2	232	239·3	43·2	119·33	184·20	−0·29	47·7
22	199·1	105·7	213	208·3	42·4	136·83	159·78	−0·26	47·0
21	221·6	117·7	190	178·3	41·4	152·33	136·86	−0·23	46·2
22·6	254·1	135	189	167·5	41	174·70	128·36	−0·22	45·9
$e = 0{\cdot}714$									
12·5	84	44·4	204	281·6	44·3	57·60	216·01	−0·32	48·5
14·1	108	57·1	197	246·6	43·4	74·07	189·37	−0·30	47·8
17	127·8	67·6	216	252·2	43·6	87·67	192·92	−0·30	47·9
19·2	148·2	78·4	222	245	43·4	101·67	187·85	−0·29	47·8
20·9	176·5	93·4	218	223·7	42·8	121·10	171·58	−0·28	47·3
21·9	201·2	106·4	211	205·5	42·3	138·00	157·70	−0·26	46·9
20·9	220·9	116·9	191	179·1	41·4	151·57	136·89	−0·23	46·2
22·6	255·5	135·2	189	167·3	41	175·30	127·92	−0·22	45·9
25·2	273·2	144·5	202	174·5	41·3	187·40	133·47	−0·23	46·1
$e = 0{\cdot}727$									
9·6	76·2	40	166	239	43·2	52·07	183·38	−0·29	47·7
10·7	98·1	51·5	159	207·7	42·4	67·03	158·62	−0·26	47·0
13·7	133·4	70	170	196·4	42	91·13	149·33	−0·25	46·7
15·8	151·3	79·3	181	198·9	42·1	103·30	151·95	−0·25	46·7
16·9	164·5	86·3	184	195·5	42	112·37	149·40	−0·25	46·7
17·6	180·9	94·9	181	185	41·6	123·57	141·43	−0·24	46·4
18·3	187·5	98·3	185	186·5	41·7	128·03	141·93	−0·24	46·4
18·2	232·2	121·8	161	149·2	40·3	158·60	113·75	−0·20	45·3
19·7	266·6	139·8	161	140·8	39·9	182·07	107·20	−0·18	45·0
$e = 0{\cdot}823$									
7·2	88·2	42·8	119	167·7	41	57·93	123·28	−0·21	45·7
8	118·8	57·6	111	138·8	39·8	78·00	101·56	−0·17	44·7
8·9	142·8	69·3	111	128·2	39·3	93·80	93·88	−0·16	44·3
9·9	183·8	89·1	106	111·1	38·4	120·67	81·04	−0·13	43·6
11·1	218·6	106	107	104·2	38	143·53	76·33	−0·12	43·3
12·1	253·9	123·1	107	98·3	37·7	166·70	71·59	−0·10	43·0

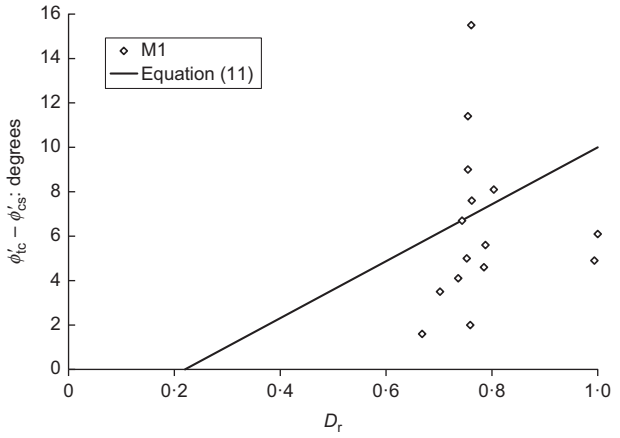

Fig. 21. Difference between peak shear resistance angles and critical state angle as a function of the relative density D_r for M1 sand

Bolton equation, reported below, is also represented as a solid line.

$$\phi'_{tc} - \phi'_{cs} = 3 \times D_r[(Q - \ln p') - R] \quad (11)$$

A very poor correlation for M1 sand can be observed.

A second point to be considered is that normally consolidated (NC) M1 sand has shown a clear dependence of the cone tip resistance q_t on the vertical effective stress σ'_v, as shown by Giretti *et al.* (2018b) in Figs 11–15. Similar behaviour has been observed by Fioravante & Giretti (2016) from centrifuge CPTs carried out in NC Ticino and Toyoura silica sands.

Jamiolkowski *et al.* (2003), analysing a very large dataset of calibration chamber CPTs in Ticino, Toyoura and Hokksund silica sands, observed that the cone penetration resistance depends on the vertical σ'_v in the case of NC sands, and the horizontal stress σ'_h plays a major role in the case of overconsolidated sands.

Recognising the importance of the horizontal stress on the cone resistance, the authors have selected the stress invariant p' for the computation of a normalised q_t.

To check and verify whether the stress-dilatancy behaviour observed for M1 is consistent with the mechanical behaviour of other carbonate sands, the authors have interpreted a series of unpublished laboratory and centrifuge tests available for Quiou sand (QS), performed at Istituto Sperimentale Modelli e Strutture (ISMES; Italy) in the 1990s.

QS is a skeletal carbonatic sand of biogenic origin (Fioravante *et al.*, 1994, 1998; Porcino *et al.*, 2008; Mesri & Vardhanabhuti, 2009).

Among the triaxial tests available for QS, Fig. 22 shows the results of selected tests which reached the critical state and allowed the definition of the QS critical state line in e–p' and q–p' planes. QS has the same ϕ'_{cs} as M1 and quite similar compressibility characteristics.

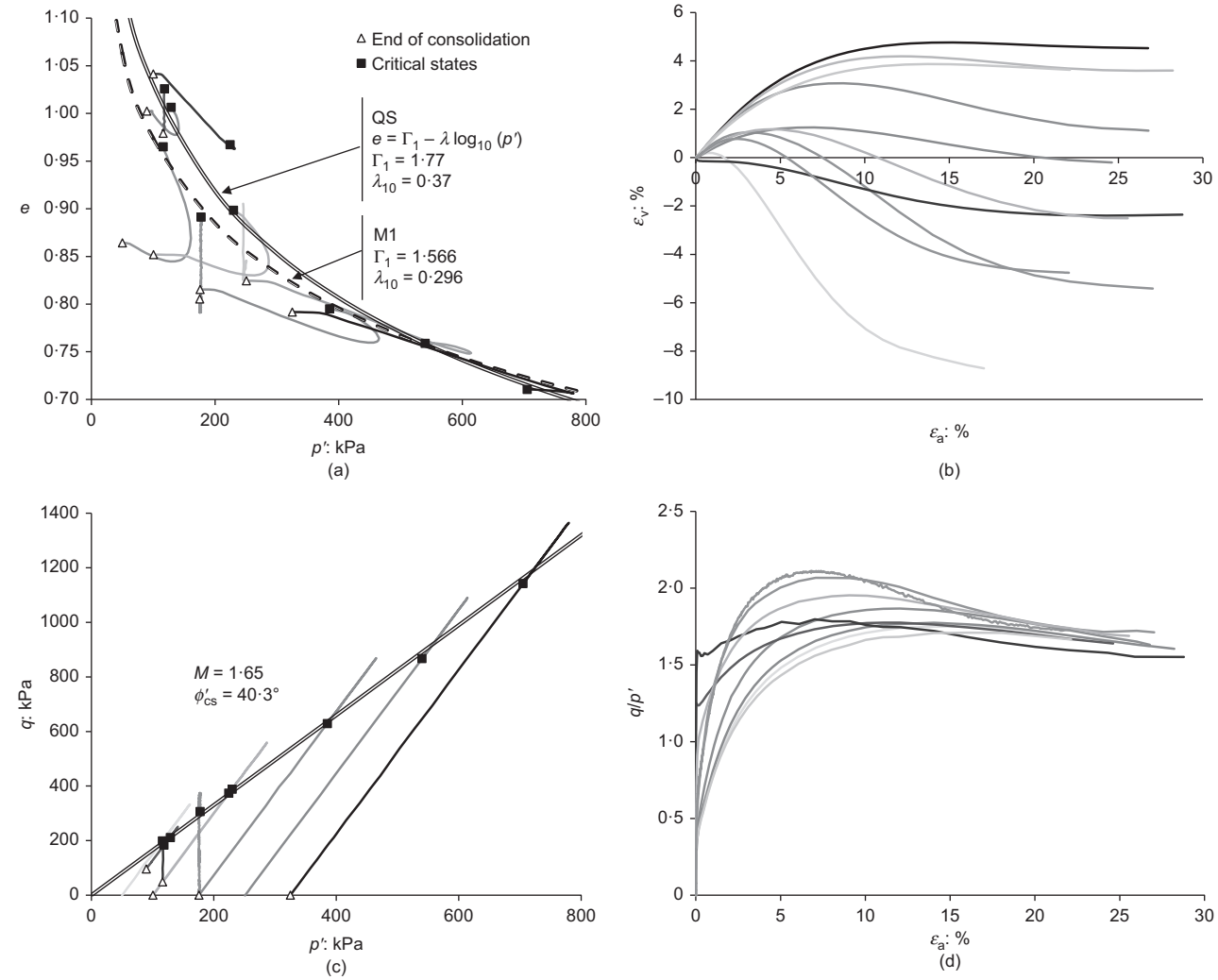

Fig. 22. Triaxial tests on QS and critical state line

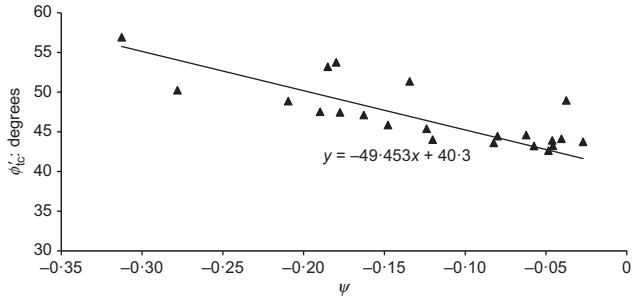

Fig. 23. QS peak shear angle ϕ'_{tc} as a function of the state parameter ψ

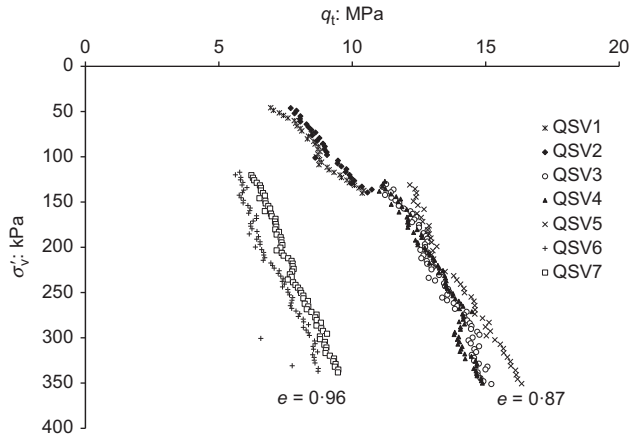

Fig. 24. Centrifuge CPTs on dry NC QS

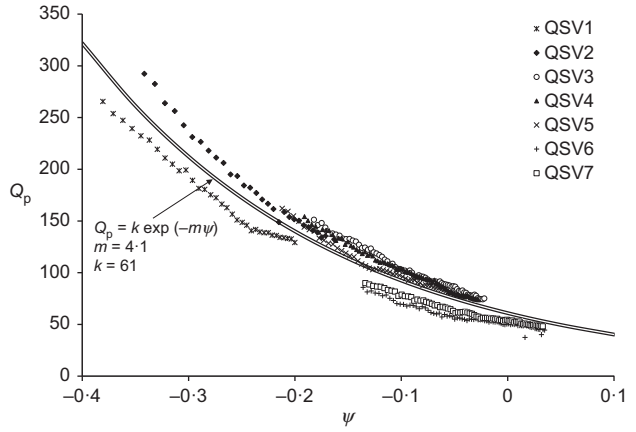

Fig. 25. State parameter interpretation of centrifuge tests on dry NC QS

Figure 23 shows the peak shear angle ϕ'_{tc} achieved in drained tests on QS as a function of the state parameter ψ at the end of consolidation. As for M1 sand, a linear relationship (equation (9)) can be used to interpolate the experimental data and the slope of the function is $a = 49{\cdot}5$.

Seven $q_t - \sigma'_v$ profiles measured on normally consolidated centrifuge models of dry QS are reported on Fig. 24. The samples have an average void ratio $e = 0{\cdot}96$ and $e = 0{\cdot}87$ and have been tested at a centrifugal acceleration of $30\boldsymbol{g}$ and $80\boldsymbol{g}$. As for M1 sand, the q_t profiles have been normalised against p' and plotted against ψ in Fig. 25. Also for QS an exponential function can be adopted to fit the experimental trends and the m and k parameters of equation (10) are 4·1 and 61, respectively.

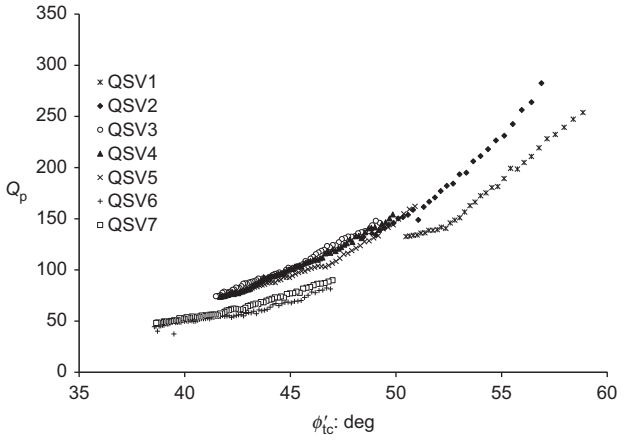

Fig. 26. Peak shear angle inferred from centrifuge CPTs on dry NC QS

Following the same procedure as M1, equations (9) and (10) have been combined to derive the peak resistance angles as a function of Q_p (see Fig. 26).

In conclusion, the state parameter ψ appears to be a useful independent state indicator to interpret the mechanical behaviour of carbonate sands.

Notation

A	parameter in equation (6)
a	fitting parameter of equation (9)
C_c	compression index, $\Delta e/\Delta \log \sigma'_v$
C_u	uniformity coefficient, D_{60}/D_{10}
D_{10}	grain size at which 10% is finer
D_{50}	mean grain size
D_{60}	grain size at which 60% is finer
D_r	relative density
e	void ratio
K_0	coefficient of earth pressure at rest
K_{0p}	coefficient of earth pressure at rest in normally consolidated young loose sands
k	fitting parameter of equation (10)
M	tangent constrained modulus, $\Delta\sigma'_v/\Delta\varepsilon_v$
M_{max}	tangent constrained modulus at the first inflection point of σ'_v plotted against ε_v
M_{min}	tangent constrained modulus at the second inflection point of σ'_v plotted against ε_v
m	fitting parameter of equation (10)
N_h	q_t/σ'_h, used in equation (8).
P_a	atmospheric pressure
p	mean total stress
p'	mean effective stress
Q	fitting parameter of equation (11)
Q_p	normalised cone resistance
q_t	cone penetration test cone resistance
R	fitting parameter of equation (11)
ε_v	vertical strain; volumetric strain
σ'_h	horizontal effective stress
σ'_v	vertical effective stress
$(\sigma'_v)_{M_{max}}$	effective vertical stress at the yield point, defined at the first inflection point of e plotted against σ'_v M_{max}
$(\sigma'_v)_{M_{min}}$	effective vertical stress at the yield point, defined at the second inflection point of e plotted against σ'_v, defining the end the second stage of compression.
$(\sigma'_v)_{MC}$	effective vertical stress at the yield point, defined at the point of maximum curvature of e plotted against σ'_v
ϕ'_{cs}	shearing resistance angle at critical state
ϕ'_{cv}	constant volume friction angle
ϕ'_p	component of friction angle resulting from interparticle interference during shear
ϕ'_{tc}	effective stress friction angle mobilised in triaxial compression
ψ	state parameter

REFERENCES

Bolton, M. D. (1986). The strength and dilatancy of sands. *Géotechnique* **36**, No. 1, 65–78, https://doi.org/10.1680/geot.1986.36.1.65.

Fioravante, V. & Giretti, D. (2016). Unidirectional cyclic resistance of Ticino and Toyoura sands from centrifuge cone penetration tests. *Acta Geotechnica* **11**, No. 4, 953–968.

Fioravante, V., Jamiolkowski, M. & Lo Presti, D. C. F. (1994). Stiffness of carbonate Quiou sand. In *Proceedings of the 13th international conference on soil mechanics and foundation engineering* (ed. Publications Committee XIII ICSMFEA), pp. 163–167. Rotterdam, the Netherlands: Balkema.

Fioravante, V., Jamiolkowski, M., Ghionna, V. N. & Pedroni, S. (1998). Stiffness of carbonate Quiou sand from CPT. In *Geotechnical site characterisation* (eds P. Robertson and P. W. Mayne), pp. 1039–1049. Rotterdam, the Netherlands: Balkema.

Giretti, D., Fioravante, V., Been, K. & Dickenson, S. (2018a). Mechanical properties of a carbonate sand from a dredged hydraulic fill. *Géotechnique* **68**, No. 5, 410–420, https://doi.org/10.1680/jgeot.16.P.304.

Giretti, D., Been, K., Fioravante, V. & Dickenson, S. (2018b). CPT calibration and analysis for a carbonate sand. *Géotechnique* **68**, No. 4, 345–357, https://doi.org/10.1680/jgeot.16.P.312.

Houlsby, G. T. & Hitchman, R. (1988). Calibration chamber tests of cone penetrometer in sand. *Géotechnique* **38**, No. 1, 39–44, https://doi.org/10.1680/geot.1988.38.1.39.

Jaky, J. (1948). Pressure in silos. *Proceedings of the 2nd international conference on soil mechanics and foundation engineering*, Rotterdam, the Netherlands, vol. 1, pp. 103–107.

Jamiolkowski, M., Lo Presti, D. C. F. & and Manassero, M. (2003). Evaluation of relative density and shear strength of sands from CPT and DMT. In *Soil behavior and soft ground construction*, (eds J. T. Germaine, T. C. Sheahan and R. V. Whitman), Geotechnical Special Publication 119, pp. 201–238, https://doi.org/10.1061/40659(2003)7. Reston, VA, USA: American Society of Civil Engineers.

Mesri, G. & Hayat, T. M. (1993). The coefficient of earth pressure at rest. *Can. Geotech. J.* **30**, No. 4, 447–666.

Mesri, G. & Vardhanabhuti, B. (2007). The coefficient of earth pressure at rest of sands subjected to vibration. *Can. Geotech. J.* **44**, No. 10, 1242–1263.

Mesri, G. & Vardhanabhuti, B. (2009). Compression of granular materials. *Can. Geotech. J.* **46**, No. 4, 369–392.

Mesri, G., Rokhsar, A. & Bohor, B. F. (1975). Composition and compressibility of typical samples of Mexico City clay. *Géotechnique* **25**, No. 3, 527–554, https://doi.org/10.1680/geot.1975.25.3.527.

Porcino, D., Caridi, G. & Ghionna, V. N. (2008). Undrained monotonic and cyclic simple shear behaviour of carbonate sand. *Géotechnique* **58**, No. 8, 635–644, https://doi.org/10.1680/geot.2007.00036.

Terzaghi, K., Peck, R. B. & Mesri, G. (1996). *Soil mechanics in engineering practice*. 3rd edn. New York, NY, USA: Wiley.